Ba(Zn,Co)_{2}As_{2}: A diluted ferromagnetic semiconductor with n-type carriers and isostructural to 122 iron-based superconductors

Shengli Guo, Huiyuan Man, Kai Wang, Cui Ding, Yao Zhao, Licheng Fu, Yilun Gu, Guoxiang Zhi, Benjamin A. Frandsen, Sky C. Cheung, Zurab Guguchia, Kohtaro Yamakawa, Bin Chen, Hangdong Wang, Z. Deng, C. Q. Jin, Yasutomo J. Uemura, and Fanlong Ning

Phys. Rev. B **99**, 155201 — Published 2 April 2019

DOI: 10.1103/PhysRevB.99.155201

$Ba(Zn,Co)_2As_2$: a Novel Diluted Ferromagnetic Semiconductor with N-type Carriers and Isostructural to "122" Iron-based Superconductors

Shengli Guo[1], Huiyuan Man[1], Kai Wang[1], Cui Ding[1], Yao Zhao[1], Licheng Fu[1], Yilun Gu[1], Guoxiang Zhi[1], Benjamin A. Frandsen[2], Sky C. Cheung[2], Zurab Guguchia[2], Kohtaro Yamakawa[2], Bin Chen[3], Hangdong Wang[3], Z. Deng[4], C.Q. Jin[4], Yasutomo J. Uemura[2] and Fanlong Ning[1,5*]

[1] *Zhejiang Province Key Laboratory of Quantum Technology and Device and Department of Physics, Zhejiang University, Hangzhou 310027, China*

[2] *Department of Physics, Columbia University, New York, New York 10027, USA*

[3] *Department of Physics, Hangzhou Normal University, Hangzhou 310016, China*

[4] *Beijing National Laboratory for Condensed Matter Physics, and Institute of Physics, Chinese Academy of Sciences, Beijing 100190, China and*

[5] *Collaborative Innovation Center of Advanced Microstructures, Nanjing University, Nanjing 210093, China*

We report the successful synthesis of a "122" diluted ferromagnetic semiconductor with n-type carriers, $Ba(Zn,Co)_2As_2$. Magnetization measurements show that the ferromagnetic transition occurs up to $T_C \sim 45$ K. Hall effect and Seebeck effect measurements jointly confirm that the dominant carriers are electrons. Through muon spin relaxation (μSR), a volume sensitive magnetic probe, we have also confirmed that the ferromagnetism in $Ba(Zn,Co)_2As_2$ is intrinsic and the internal field is static.

PACS numbers: 75.50.Pp, 76.75.+i, 75.50.Lk, 77.80.B-

I. INTRODUCTION

The combination of spin and charge degrees of freedom in diluted magnetic semiconductors (DMSs) makes them promising materials for spintronics. The observation of ferromagnetism in Mn doped III-V GaAs has therefore attracted extensive attention in the last two decades[1–4]. (Ga,Mn)As films are typically fabricated via low-temperature molecular beam epitaxy (LT-MBE), where substitution of Mn^{2+} for Ga^{3+} introduces both spins and holes simultaneously. Despite the controversy about the origin of ferromagnetism in (Ga,Mn)As[5], it has been widely accepted that the itinerant carriers mediate the ferromagnetic interaction between spatially separated magnetic ions. To date, the Curie temperature T_C in (Ga,Mn)As has a maximum value of $\sim$ 190-200 K[6–8], which is still far below room temperature and therefore limits the possibilities for practical applications. Recently, a series of DMS materials that are structural derivatives of iron-based superconductors have been synthesized, including I-II-V Li(Zn,Mn)As[9], "1111" (La,Ba)(Zn,Mn)AsO[10] and "122" $(Ba,K)(Zn,Mn)_2As_2$[11]. Of these, $(Ba,K)(Zn,Mn)_2As_2$ has T_C as high as 180 K[11]. $(Ba,K)(Zn,Mn)_2As_2$ was synthesized through the doping of K and Mn into the parent semiconductor $BaZn_2As_2$, where the substitution of Mn for Zn introduces magnetic moments and the substitution of K for Ba introduces carriers. Considering that the end member $BaMn_2As_2$ is an antiferromagnet with a Neel temperature of 625 K[12], it seems possible that T_C may reach room temperature in "122" systems when the synthesis conditions and the selection of elements are optimzed[13].

The above-mentioned DMSs are all p-type, i.e., the dominant carriers are holes. N-type DMSs with electron carriers are still exceptionally rare. In practical applications, both p- and n-type DMSs are required to fabricate junctions and devices. Furthermore, n-type DMSs may shed light on the general mechanism for ferromagnetic ordering in DMSs. In the past, Co:ZnO films have been proposed to be a candidate for n-type DMS[14–16]. However, the underlying mechanism is still under debate. For example, careful investigations showed that the ferromagnetism may arise from a hydrogen-facilitated interaction[17], metallic clusters[18,19], uncompensated spins at the surface of Co-rich antiferromagnetic nanocrystals[20] or bound magnetic polarons[21]. Co:TiO_2 films are also reported to possess ferromagnetism above room temperature, with electrons provided by defects or electric fields acting as carriers[22,23]. A depth resolved low-energy μSR investigation showed that Co:TiO_2 is fully magnetic with intrinsic ferromagnetism[24]. Recently, Hai *et. al.* reported the observation of electron-mediated ferromagnetism in (In,Fe)As films where interstitial Be provides electrons[25–27]. Similar fabrication routes have also been tried in (In,Co)As films, but no ferromagnetic ordering has been observed[28]. Very recently, ferromagnetism above room temperature has also been reported in p-type (Ga,Fe)Sb and (In,Fe)Sb[29,30]. Theoretically, Gu *et. al.* predicted that n-type DMSs may be realized in narrow-band-gap semiconductors[31].

In this paper, we demonstrate the successful synthesis of a high-quality n-type ferromagnetic semiconductor by doping Co onto the Zn sites of the narrow-band-gap (0.2 eV) semiconductor $BaZn_2As_2$[32]. The highest T_C of $Ba(Zn_{1-x}Co_x)_2As_2$ reaches $\sim$ 45 K for $x = 0.04$. Using muon spin relaxation (μSR) measurements, we have confirmed the homogeneous and intrinsic nature of the ferromagnetic ordering in $Ba(Zn,Co)_2As_2$.

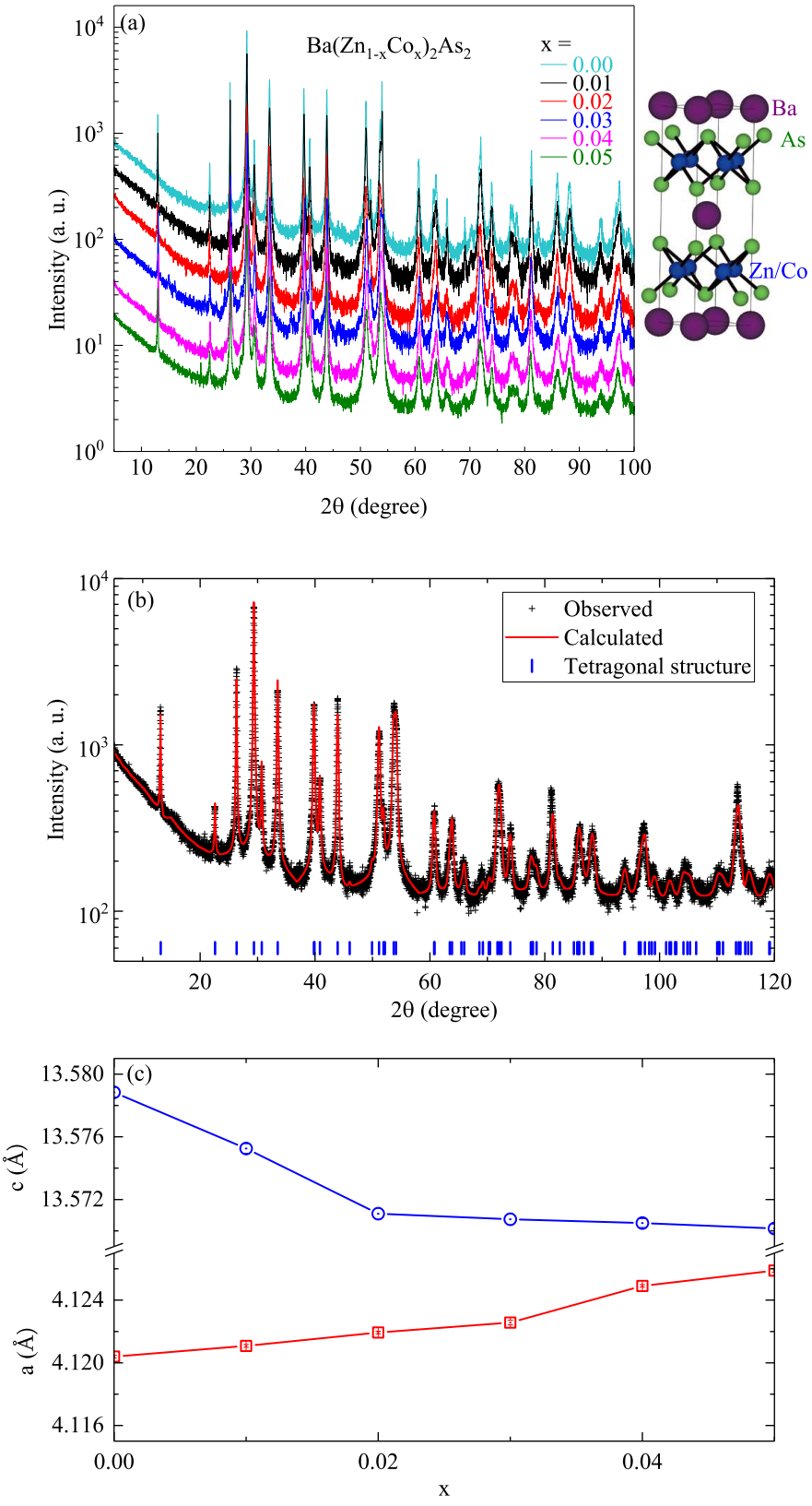

Figure 1: Structural and X-ray diffraction results. (a) X-ray diffraction patterns of $Ba(Zn_{1-x}Co_x)_2As_2$ with different doping levels on a semi-log scale. The diffraction patterns of $Ba(Zn_{1-x}Co_x)_2As_2$ with $x = 0.01, 0.02, 0.03, 0.04, 0.05$ are shifted downwards for clarify. (b) Rietveld refinement profile for $x = 0.04$ on a semi-log scale. (c) Lattice parameters of $Ba(Zn_{1-x}Co_x)_2As_2$.

II. EXPERIMENTAL METHODS

A. Material synthesis.

Polycrystalline samples of $Ba(Zn,Co)_2As_2$ were synthesized via a solid state reaction of high purity elements ($\geq$ 99.9%) Ba, Zn, Co and As. Mixed ingredients were placed in alumina crucibles and sealed in evacuated silica tubes. All handling of the elements was conducted in a glove box filled with high purity Ar (the content of H_2O and O_2 is less than 0.1 ppm) except for the sealing of the silica tubes. The mixture was heated to 900 °C for 10 h, then held at 1150 °C for 24 h followed by cooling in the furnace. The products were then ground, pressed into pellets, sealed in evacuated silica tubes, and subsequently heated to 1150 °C and held for over 24 hours followed by fast cooling to keep the tetragonal phase.

B. Structural characterization.

Powder X-ray diffraction was performed at room temperature using a PANalytical X-ray diffractometer (Model EMPYREAN) with monochromatic Cu-$K_{\alpha 1}$ radiation. Energy-dispersive X-ray spectroscopy (EDX) was measured using a field emission scanning microscope (Model FEI SIRION-100).

C. Experimental characterization

DC magnetization measurements were conducted using a Quantum Design Magnetic Property Measurement System (MPMS3). The Hall effect and magnetoresistivity were measured using a Quantum Design Physical Property Measurement System (PPMS). The Seebeck coefficient was measured at room temperature using a commercial thermopower measurement apparatus. The zero field resistivity was measured via the typical four-probe method with a Keithley 6221 DC and AC current source and Keithley 2182A nanovoltmeter. μSR measurements were performed using the LAMPF spectrometer on the M20 beamline at TRIUMF, Canada, and μSR data were analyzed using the musrfit package[33].

III. RESULTS AND DISCUSSION

A. X-ray diffraction.

In Fig. 1(a), we show the X-ray diffraction patterns for $Ba(Zn_{1-x}Co_x)_2As_2$ with different doping levels. In general, $BaZn_2As_2$ is polymorphic, typically crystallizing in either an orthorhombic structure (space group *Pnma*) or a tetragonal structure (space group *I4/mmm*)[11]. The tetragonal structure results in a semiconductor with a band gap of $\sim$ 0.2 eV[32] that forms the parent compound of the $(Ba,K)(Zn,Mn)_2As_2$ DMS system. In this structure, layers of $\{ZnAs_4\}$ tetrahedra stack alternately with Ba layers along the c axis. We note that if the Zn atoms are replaced by Fe, the resulting material $BaFe_2As_2$ is the parent compound of many iron based superconductors[34]. The X-ray diffraction peaks in Fig. 1(a) can be well indexed with a tetragonal structure (space group *I4/mmm*) with no sign of the orthorhombic phase or other impurities. In Fig. 1(b), we show the Rietveld refinement profile for the $x = 0.04$ sample using the GSAS-II package[35]. No obvious impurity peaks were observed, and the resulting weighted reliability factor R_{wp} is $\sim$ 9.87%, indicating a high sample quality. In Fig. 1(c), we show the lattice parameters of different doping levels. With increasing Co concentration a increases and c decreases monotonically. The monotonic behavior of the lattice parameters indicates the successful doping of Co up to $x = 0.05$. Higher doping does not produce a pure phase, which is also the reason why the resistivity of the $x = 0.05$ sample is larger than that of the $x = 0.04$ sample (see Fig. 5(a)).

Table I: The atomic percentages of Ba, Zn, Co and As in $Ba(Zn_{1-x}Co_x)_2As_2$ with $x = 0.04$.

	Ba (%)	Zn (%)	Co (%)	As (%)
First	20.93	34.99	1.68	42.40
Second	20.81	37.28	1.67	40.23
Third	24.33	36.53	1.68	40.03
Average	22.02	36.27	1.68	40.03

B. Energy-dispersive X-ray spectroscopy

In Fig. 2, we show the surface morphology under scanning electron microscopy (SEM) and the energy spectroscopy of energy-dispersive X-ray spectroscopy (EDX) for $Ba(Zn_{1-x}Co_x)_2As_2$ with $x = 0.04$. We select three different areas on the same sample and take the average results as the elemental composition. In Fig. 2(b), we show a typical EDX spectrum. Besides the low energy peaks which come from the elements C and O adhered on the surface, the other peaks are all indexed by Ba, Zn, Co and As. We tabulated the atomic percentages in Table. I. The ratio of Ba:(Co+Zn):As is close to the chemical formula, and the Co concentration, the ratio of Co:(Co+Zn), is $\sim$ 4.4%, which is consistent with our nominal doping level.

C. Magnetic properties.

In Fig. 3(a), we show the temperature-dependent magnetization of $Ba(Zn_{1-x}Co_x)_2As_2$ ($x = 0.01, 0.02, 0.03, 0.04, 0.05$) in an applied magnetic field of 100 Oe. Zero field cooling (ZFC) and

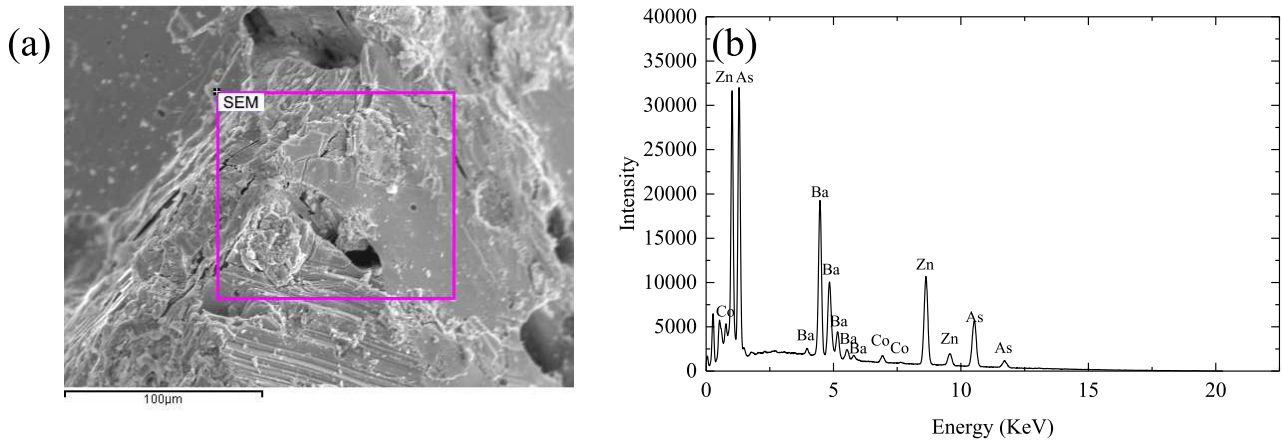

Figure 2: SEM and EDX of $Ba(Zn_{1-x}Co_x)_2As_2$ with $x = 0.04$. (a) The surface morphology within the length scale of 100 nm. The rectangle is the test area for EDX. (b) The energy spectroscopy of EDX. The characteristic peaks of Ba, Zn, Co and As have been marked. Note that the peaks at low energy come from C and O atoms.

Table II: Curie temperature (T_C), Weiss temperature and effective moment (θ and μ_{eff}, derived from Curie-Weiss fitting), saturation moment (μ_s, the value measured at $T = 2$ K and $H = 200$ Oe), coercive field (H_c)

Co concentration (x)	T_C (K)	θ (K)	μ_{eff} (μ_B/Co)	μ_s (μ_B/Co)	H_c (Oe)
0.01	/	0.03	2.0	/	/
0.02	35	53	1.1	0.18	16
0.03	37	54	1.7	0.20	22
0.04	45	57	1.4	0.24	6
0.05	41	51	1.4	0.22	11

field cooling (FC) data are represented by open and filled symbols, respectively. For $x = 0.01$, no magnetic transition was observed down to the base temperature of 2 K, and the magnetic moment at 2 K in $H = 100$ Oe is only 0.005 μ_B/Co. However, for Co concentrations exceeding 1%, a sudden increase of the magnetization develops around 35-45 K, indicative of a ferromagnetic transition.

We used the Arrott plot method for the precise determination of the Curie temperature T_C for $Ba(Zn_{1-x}Co_x)_2As_2$[36]. In Fig. 3(e), we show the Arrott plot for $x = 0.05$. Around T_C, the points in high magnetic field fall approximately on a series of parallel lines. The solid lines displayed on the plot are the linear fits at high magnetic field, and the nonlinear behavior at low field is ascribed to the higher-order terms we omitted from the analysis or other deviations from mean field theory. We identify T_C as 41 K, the temperature at which the parallel line would pass through the origin. T_C for other doping levels was also determined by this method (see Supplement)[37]. We list T_C for $Ba(Zn_{1-x}Co_x)_2As_2$ in Table II. We also obtained the effective moments μ_{eff} by fitting the temperature dependent magnetization above T_C with a modified Curie-Weiss law: $\chi = \chi_0 + C/(T-\theta)$, where χ_0 is the temperature independent component, C is the Curie constant and θ is the Weiss temperature. μ_{eff} is $\sim$ 1.1-1.7 μ_B/Co. According to $\mu_{eff} = \mu_B g\sqrt{S(S+1)}$, where μ_B is the Bohr magneton and assuming the Lande factor $g = 2$, we estimate the average spin state of Co to be close to S = 1/2. Due to the contribution of holes and interstitial Mn, the magnetic moment of Mn in (Ga,Mn)As from magnetization measurements has also been reported to be less than the expected value of $5\mu_B$/Mn[38,39].

In Fig. 3(b), we show the isothermal magnetization at 2 K. Clear hysteresis loops are observed for all doping levels except the paramagnetic $x = 0.01$ sample. The coercive field of $Ba(Zn,Co)_2As_2$ is on the order of $\sim$ 10 Oe, which is much smaller than the value of 1 T in $(Ba,K)(Zn,Mn)_2As_2$[11]. The small coercive field is consistent with the minimal bifurcation of ZFC and FC curves at 100 Oe shown in Fig. 3(a). In Fig. 3(c), we show the temperature dependence of the hysteresis loop for $x = 0.04$. With increasing the temperature, the moment become smaller and the hysteresis loop eventually disappears above 50 K. The saturation moment (μ_s) is $\sim$ 0.2 - 0.3 μ_B/Co for $Ba(Zn,Co)_2As_2$ which is much smaller than 2 μ_B/Mn for $(Ba,K)(Zn,Mn)_2As_2$ and 5 μ_B/Mn for (Ga,Mn)As[2,11].

D. Hall effect, Seebeck effect and transport.

We jointly utilized measurements of the Hall effect and Seebeck effect (see Supplement) to investigate the properties of the carriers[37]. Since $R_{Hall} = B/(ne)$, where B is the external field perpendicular to the current and e is the elementary charge, we obtained the carrier con-

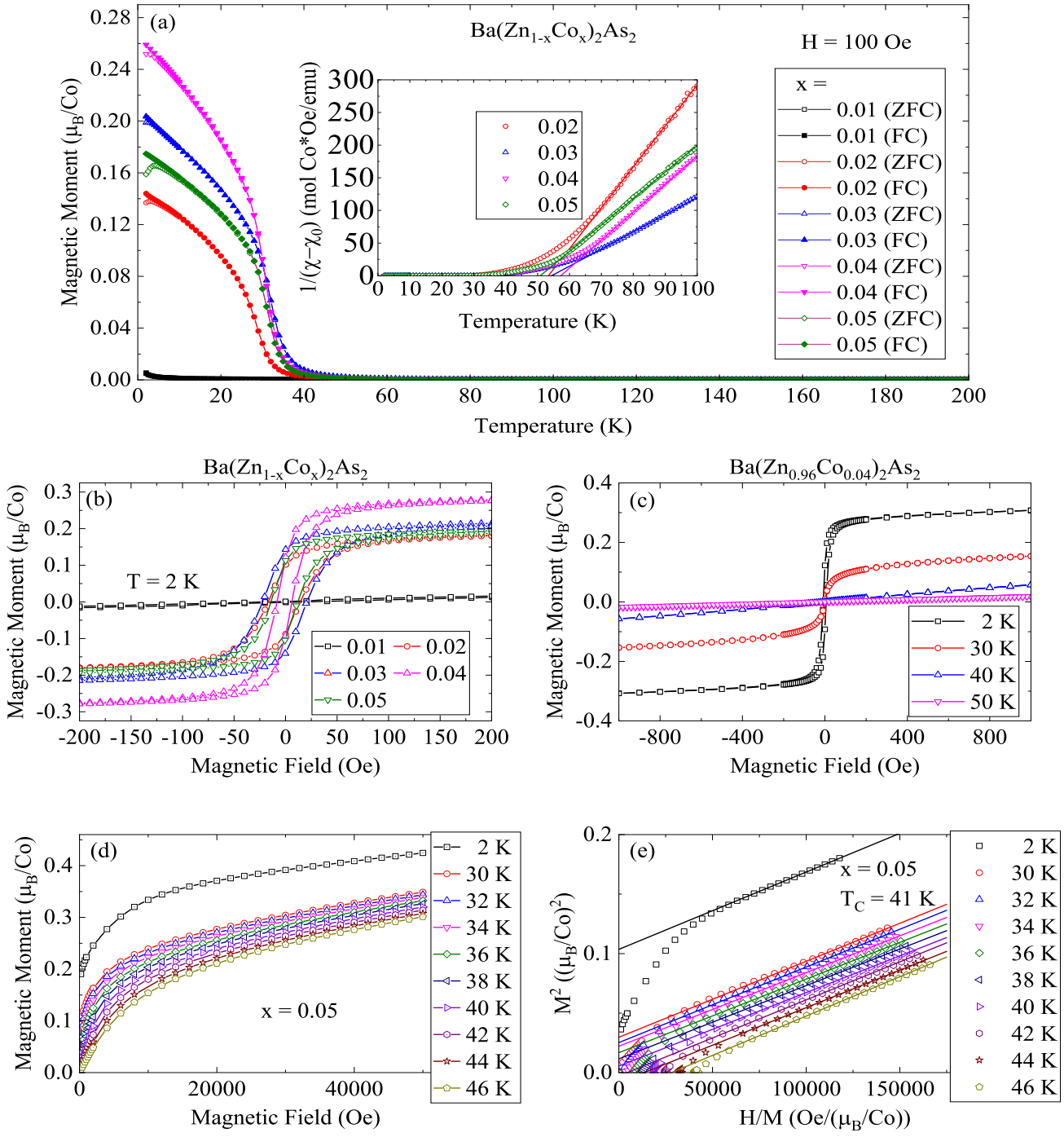

Figure 3: Magnetization results. (a) The temperature-dependent magnetization of $Ba(Zn_{1-x}Co_x)_2As_2$ ($x = 0.01, 0.02, 0.03, 0.04, 0.05$) in a magnetic field of 100 Oe. The open and filled symbols represent the zero-field-cooled and field-cooled data, respectively. Inset: Plot of $1/(\chi - \chi_0)$ versus T. Straight lines represent a Curie-Weiss fit. (b) The isothermal magnetization of $Ba(Zn_{1-x}Co_x)_2As_2$ ($x = 0.01, 0.02, 0.03, 0.04, 0.05$) at 2 K in an applied magnetic field ranging from -200 Oe to 200 Oe. (c) Evolution of the hysteresis loop of $Ba(Zn_{0.96}Co_{0.04})_2As_2$ with increasing temperature. (d) Isothermal magnetization of $Ba(Zn_{0.95}Co_{0.05})_2As_2$ at different temperatures. (e) The Arrott plot for $Ba(Zn_{0.95}Co_{0.05})_2As_2$ at different temperatures. Lines show the best linear fit.

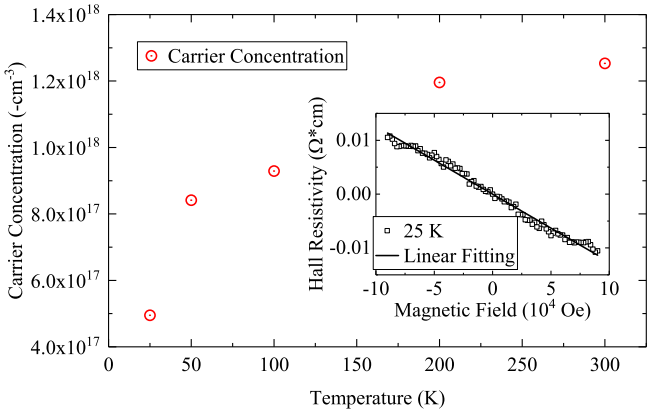

Figure 4: Results of Hall effect measurements. Carrier concentration of $Ba(Zn_{0.96}Co_{0.04})_2As_2$ calculated from Hall resistivity curves. The inset displays the Hall resistivity at 25 K, with a linear fit shown by the line.

centration from R_{Hall} versus B curves. In Fig. 4, we show the representative Hall resistivity (R_H) at 25 K and the variation of carrier density (n) versus temperature (T). Ideally, we should observe the anomalous Hall effect below T_C, but the signal to noise ratio is poor in the measurement. Nonetheless, the negative slope of the Hall resistivity curve indicates that the dominant carriers in $Ba(Zn,Co)_2As_2$ are electrons. The carrier concentration is roughly estimated to be $10^{17} \sim 10^{18}/cm^{-3}$ depending on the measured temperature. This low carrier concentration is comparable to that of Li(Zn,Mn)P and indicates that the electrons introduced by Co doping are mostly localized[40]. The carrier density decreases gradually with decreasing temperature. Seebeck effect measurements at room temperature were also conducted to investigate the carrier type (see Supplement)[37]. The Seebeck coefficient is $S = -\Delta U/\Delta T$, where ΔU is the voltage difference between two electrodes and ΔT is the temperature difference. The sign of the Seebeck coefficient is related to the carrier type, positive for p-type carriers and negative for n-type carriers. The room temperature Seebeck coefficient is $\sim$ -16 μV/K for $x = 0.04$ and $\sim$ -7 μV/K for $x = 0.05$. The negative Seebeck coefficient confirms our conclusion of n-type carriers.

In Fig. 5(a), we show the electrical transport properties for different doping levels. With Co doping, the resistivity retains its semiconducting behavior but the magnitude decreases, indicating the successful introduction of carriers by Co substitution for Zn. In Fig. 5(b), we show the resistivity in different magnetic fields (R(H)) for the $x = 0.04$ sample. The R(H) curve decreases clearly below T_C, which is due to the suppression of magnetic scattering by the external field. At $T = 2$ K, R(H) reaches a minimum at $H = 6000$ Oe with $(\rho - \rho(0))/\rho(0)$ reaching $\sim -17\%$, as shown in the inset of Fig. 5(b). This value is much larger than the value of $\sim 7.5\%$ for $(Ba,K)(Zn,Mn)_2As_2$ at 7 T[41]. Above 6000 Oe, R(H)

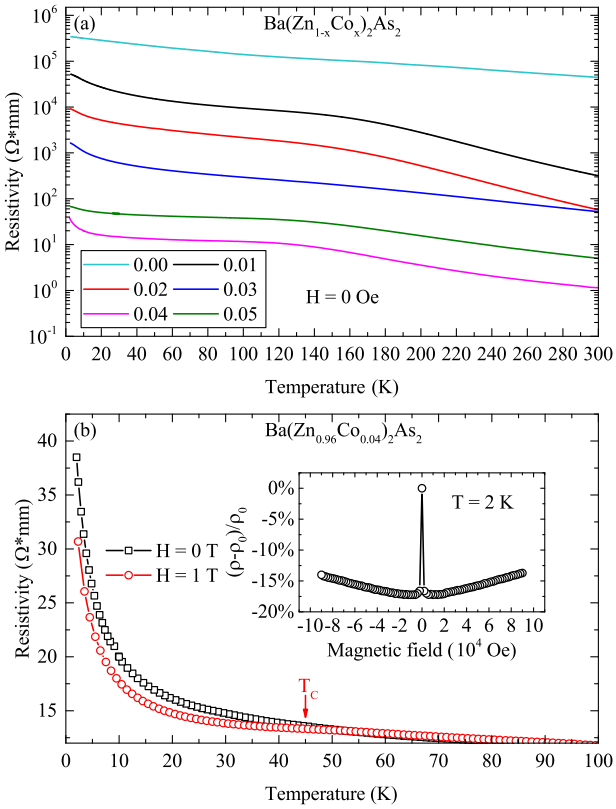

Figure 5: Results of resistivity measurements. (a) The resistivity as a function of temperature for different doping levels. (b) The temperature dependence of the resistivity for the $x = 0.04$ sample under 0 T and a 1 T magnetic field. The red arrow marks the position of $T_C \sim 45$ K. The inset shows $(\rho - \rho(0))/\rho(0)$ measured at 2 K, with a field interval of 2000 Oe.

displays a slight increase with increasing external field. This positive R(H) is from the field-induced spin splitting on disorder-modified electron-electron interactions that has been observed in n-type (Zn,Co)O[20]. Nonetheless, the high sensitivity of the resistivity to magnetic field indicates that the electrical transport properties of $Ba(Zn,Co)_2As_2$ can be easily controlled by external magnetic field.

E. ZF- and LF-μSR.

Generally speaking, a small amount of magnetic impurities such as Co nanoparticles or unknown Co compounds can give rise to magnetic signals, which may obscure the intrinsic magnetic properties. To rule out such a scenario, we performed μSR, a volume-sensitive magnetic probe, to investigate $Ba(Zn,Co)_2As_2$. In Fig. 6(a), we show the zero field (ZF-) μSR time spectra for $Ba(Zn_{0.95}Co_{0.05})_2As_2$. A fast-relaxing component clearly arises below T_C, consistent with the formation

Table III: Comparison of selected properties of (Ga,Mn)As, (Ba,K)(Zn,Mn)$_2$As$_2$ and Ba(Zn,Co)$_2$As$_2$.

	(Ga,Mn)As	(Ba,K)(Zn,Mn)$_2$As$_2$	Ba(Zn,Co)$_2$As$_2$
Valence before doping	III-V	II-II-V	II-II-V
Carrier type	holes	holes	electrons
Maximum T_C	190 K[6]	180 K[11]	45 K
Saturation moment	5 μ_B/Mn	2 μ_B/Mn	0.2 μ_B/Co
Sample form	thin film	bulk form	bulk form

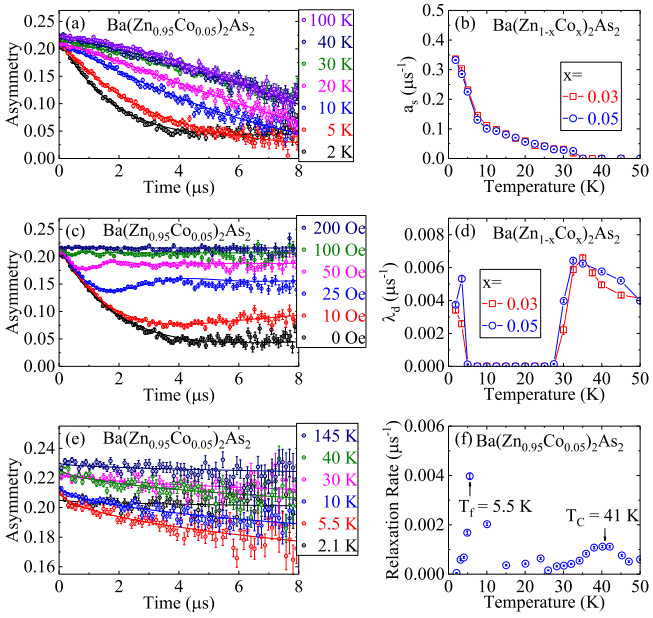

Figure 6: Results of μSR characterization.(a) ZF-μSR time spectra of Ba(Zn$_{0.95}$Co$_{0.05}$)$_2$As$_2$. The solid lines show the best fit to the dynamic-static relaxation function with the static local field amplitude parameter a_s shown in (b) and the dynamic relaxation rate parameter λ_d shown in (d). The LF-μSR time spectra are shown in (c), exhibiting full decoupling at 200 Oe. (e) The time spectra of LF-μSR in Ba(Zn$_{0.95}$Co$_{0.05}$)$_2$As$_2$ with an external field of 100 Oe at different temperatures. (f)The muon spin relaxation rate 1/T$_1$.

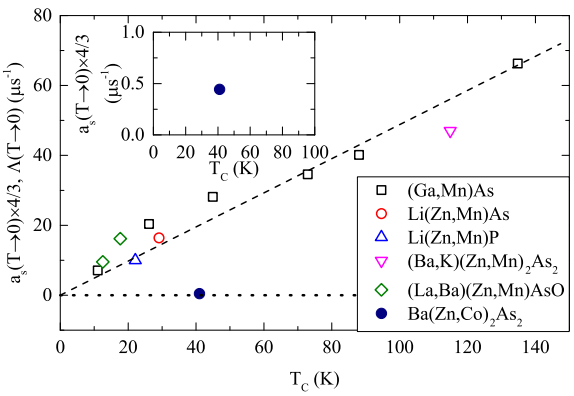

Figure 7: Plot of a_s versus T_C. Correlation between the static internal field parameter a_s determined at $T = 2$ K by ZF-μSR versus the ferromagnetic Curie temperature T_C observed in (Ga,Mn)As[43], Li(Zn,Mn)As[9], Li(Zn,Mn)P[44], (La,Ba)(Zn,Mn)AsO[10], (Ba,K)(Zn,Mn)$_2$As$_2$[11], and Ba(Zn,Co)$_2$As$_2$ (current study). A factor 4/3 is multiplied to the parameter a_s to adjust the difference from the simple exponential decay rate Λ adopted in (Ga,Mn)As[43].

of ferromagnetic order. Similar to the case of p-type "1111" DMS systems (La,Ba)(Zn,Mn)AsO[10], we use a dynamic spin freezing model to fit the ZF-μSR data. As shown by the solid curves in Fig. 6(a), the time spectra can be well fitted by the dynamic-static relaxation function: $A(t) = A_s\{\frac{1}{3}exp[-(\lambda_d t)^{1/2}] + \frac{2}{3}[1 - \frac{a_s^2 t^2}{(\lambda_d t + a_s^2 t^2)^{1/2}}]exp[-(\lambda_d t + a_s^2 t^2)^{1/2}]\}g_z(t)$, in which $g_z(t) = \frac{1}{3} + \frac{2}{3}(1-\Delta^2 t^2)exp(-\frac{1}{2}\Delta^2 t^2)$ is the static Gaussian Kubo-Toyabe function that describes the nuclear contribution. This indicates that Ba(Zn$_{0.95}$Co$_{0.05}$)$_2$As$_2$ achieves static magnetic order throughout the entire volume at low temperatures, confirming that the previous magnetization measurements are intrinsic to the samples and not due to a small impurity phase. The static internal field parameter a_s that is related to the time/frequency window of the probe (muon) and the dynamic relaxation rate λ_d determined from the fits are displayed in Fig. 6(b) and (d). The parameter a_s is proportional to the individual ordered moment size multiplied by the moment concentration. a_s is zero above T_C, and starts to increase below T_C, indicating the emergence of a static field in the ferromagnetic state.

We used longitudinal field (LF-)μSR to investigate the spin dynamics in Ba(Zn,Co)$_2$As$_2$. In Fig. 6(c), we show the field dependence of the LF-μSR spectra measured at 2 K. An external field of $\sim$ 100 Oe fully decouples the LF-μSR time spectra, indicating that the internal magnetic field at the muon stopping sites is fully static and has a magnitude about 10 times less than the decoupling field, i.e. $\sim$ 10 Oe. In Fig. 6(e), we show the temperature-dependent LF-μSR spectra conducted under a constant external field of 100 Oe and plot the extracted relaxation rate 1/T$_1$ in Fig. 6(f). 1/T$_1$ displays similar behavior as λ_d obtained from ZF-μSR(Fig. 6(d)). The dynamic relaxation exhibits two peaks, one corresponding to T_C arising from the critical slowing down of spin fluctuations near T_C, and the other arising at the temperature where

ZFC and FC curves start to bifurcate as shown in Fig. 3(a). This temperature should be related to the freezing of magnetic domains.

F. Discussion

When we plot the static internal field parameter a_s versus T_C in Fig. 7, the point for the present n-type system lies at a location very different from the linear trend shown by many other p-type DMS systems[9–11,43,44]. Since the static internal field parameter a_s is proportional to the concentration multiplied by the average static moment size in dilute spin systems, the trend for the n-type system implies that T_C is relatively high for the given size and density of the static ordered moments. This tendency can be partly ascribed to the difference between the present Co-doped system and Mn-doped p-type "122" DMS systems, which involve frustration. This is because the nearest-neighbor Mn pairs are coupled antiferromagnetically, as can be seen in $BaMn_2As_2$ being a strong antiferromagnet with $T_N \sim 625$ K[12]. In contrast, $BaCo_2As_2$ is a paramagnet showing a tendency towards ferromagnetic correlations[45,50]. Therefore, there is no frustration between neighboring Co spins in the Co-doped "122" system. This could lead to the smaller coercive field and stronger ferromagnetic coupling in the n-type system compared to the p-type Mn doped DMS system. This feature may be helpful for obtaining higher T_C in n-type DMS systems. Another concern we should note is the superparamagnetic-like fragments caused by the fluctuations of the carrier density[46–49]. If the dynamic frequency of these superparamagnetic-like fragments is smaller than the lower frequency limit of μSR that is $\sim 10^4$ Hz, μSR will treat them static.

The n-type DMS $Ba(Zn,Co)_2As_2$ (T_C = 45 K) from the current study joins several related compounds including the p-type DMS $(Ba,K)(Zn,Mn)_2As_2$ (T_C = 180 K, see Table III)[11], the Fe-based superconductor $Ba(Fe,Co)_2As_2$ (T_c = 25 K)[34], the antiferromagnetic insulator $BaMn_2As_2$ (T_N = 625 K)[12], and the paramagnetic metal $BaCo_2As_2$[50]. They all share a common tetragonal crystal structure with a lattice mismatch of less than 5%. Superconducting films of $Ba(Fe_{1-x}Co_x)_2As_2$ have been fabricated successfully using pulsed laser deposition methods by many groups[51]. Recently, Xiao *et al* have successfully grown high-quality epitaxial films of the tetragonal β-$BaZn_2As_2$[32], and Cao *et al* are working on the growth of $Ba(Zn,Co)_2As_2$ films[52]. With the progress of thin film growth, it is conceivable that various junctions and devices can be fabricated to combine n-type DMS $Ba(Zn,Co)_2As_2$, p-type DMS $(Ba,K)(Zn,Mn)_2As_2$, and the superconductor $Ba(Fe,Co)_2As_2$ through the As layers.

IV. CONCLUSION

We have successfully synthesized the ferromagnetic semiconductor $Ba(Zn,Co)_2As_2$ via the solid state reaction method. Hall resistivity and Seebeck coefficient measurements jointly confirmed that the carriers in $Ba(Zn_{1-x}Co_x)_2As_2$ are electrons. Magnetization measurements show that the highest T_C is $\sim$ 45 K for the 4% doping level and the coercive field is on the order of 10 Oe. ZF- and LF-μSR measurements show that a static field arises throughout the full sample volume below T_C, with a magnitude of about 10 Oe at the muon stopping sites. In the temperature-dependent LF-μSR measurements, we observe a critical slowing down of spin fluctuations around T_C and the freezing of magnetic domains at a lower temperature. Combining the ZF- and LF-μSR time spectra, we conclude that the present n-type DMS system exhibits characteristic signatures of dynamic slowing down followed by static magnetic order, with a magnetically ordered state in the entire volume within the time/frequency window.

Acknowledgments

The work at Zhejiang was supported by MOST (No. 2016YFA0300402), NSF of China (11574265), NSF of Zhejiang Province (No. LR15A040001 and No. LY14A040007) and the Fundamental Research Funds for the Central Universities; at Columbia by NSF (DMR 1610633 and DMREF DMR-1436095) and thank JAEA Reimei project; at IOPCAS by NSF & MOST through research projects. F.L. Ning acknowledge helpful discussions with B. Gu, S. Maekawa, Kaiyou Wang, Hanoh Lee, Igor Mazin, Igor Zutic and Jianhua Zhao, and the help from Gerald D. Morris, Bassam S. Hitti and other staffs in the process of μSR measurements at TRIUMF.

* Electronic address: ningfl@zju.edu.cn

[1] H. Ohno, A. Shen, F. Matsukura, A. Oiwa, A. Endo, S. Katsumoto, and Y. Iye, Appl. Phys. Lett. **69**, 363 (1996).
[2] H. Ohno, Science **281**, 951 (1998).
[3] I. Zutic, J. Fabian, and S. Das Sarma, Rev. Mod. Phys. **76**, 323 (2004).
[4] T. Jungwirth, J. Sinova, J. Masek, J. Kucera, and A. H. MacDonald, Rev. Mod. Phys. **78**, 809 (2006).
[5] T. Dietl and H. Ohno, Rev. Mod. Phys. **86**, 187 (2014).
[6] M. Wang, R. P. Campion, A. W. Rushforth, K. W. Edmonds, C. T. Foxon, and B. L. Gallagher, Appl. Phys. Lett. **93**, 132103 (2008).
[7] L. Chen, S. Yan, P. F. Xu, J. Lu, W. Z. Wang, J. J. Deng, X. Qian, Y. Ji, and J. H. Zhao, Appl. Phys. Lett. **95**, 182505 (2009).
[8] L. Chen, X. Yang, F. Yang, J. Zhao, J. Misuraca, P. Xiong, and S. von Molnar, Nano. Lett. **11**, 2584 (2011)
[9] Z. Deng, C. Q. Jin, Q. Q. Liu, X. C. Wang, J. L. Zhu, S. M.

Feng, L. C. Chen, R. C. Yu, C. Arguello, T. Goko, F. Ning, J. Zhang, Y. Wang, A. A. Aczel, T. Munsie, T. J. Williams, G. M. Luke, T. Kakeshita, S. Uchida, W. Higemoto, T. U. Ito, B. Gu, S. Maekawa, G. D. Morris, and Y. J. Uemura, Nat. Commun. **2**, 422 (2011).

[10] C. Ding, H. Man, C. Qin, J. Lu, Y. Sun, Q. Wang, B. Yu, C. Feng, T. Goko, C. J. Arguello, L. Liu, B. A. Frandsen, Y. J. Uemura, H. Wang, H. Luetkens, E. Morenzoni, W. Han, C. Q. Jin, T. Munsie, T. J. Williams, R. M. D'Ortenzio, T. Medina, G. M. Luke, T. Imai, and F. L. Ning, Phys. Rev. B **88**, 041102(R) (2013).

[11] K. Zhao, Z. Deng, X. C. Wang, W. Han, J. L. Zhu, X. Li, Q. Q. Liu, R. C. Yu, T. Goko, B. Frandsen, L. Liu, F. Ning, Y. J. Uemura, H. Dabkowska, G. M. Luke, H. Luetkens, E. Morenzoni, S. R. Dunsiger, A. Senyshyn, P. Boni, and C. Q. Jin, Nat. Commun. **4**, 1442 (2013).

[12] Y. Singh, M. A. Green, Q. Huang, A. Kreyssig, R. J. McQueeney, D. C. Johnston, and A. I. Goldman, Phys. Rev. B **80**, 100403(R) (2009).

[13] A. Hirohata, H. Sukegawa, H. Yanagihara, I. Zutic, T. Seki, S. Mizukami, and R. Swaminathan, IEEE Trans. Magn. **51**, 1 (2015).

[14] K. Sato and H. Katayama-Yoshida, Physica E **10**, 251 (2001).

[15] M. Venkatesan, C. B. Fitzgerald, J. G. Lunney, and J. M. D. Coey, Phys. Rev. Lett. **93**, 177206 (2004).

[16] D. A. Schwartz and D. R. Gamelin, Adv. Mater. **16** 2115 (2004).

[17] L. Li, Y. Guo, X. Y. Cui, R. Zheng, K. Ohtani, C. Kong, A. V. Ceguerra, M. P. Moody, J. D. Ye, H. H. Tan, C. Jagadish, H. Liu, C. Stampfl, H. Ohno, S. P. Ringer, and F. Matsukura, Phys. Rev. B **85**, 174430 (2012).

[18] R. Boubekri, Z. Beji, K. Elkabous, F. Herbst, G. Viau, S. Ammar, F. Fievet, H. J. von Bardeleben, and A. Mauger, Chem. Mater. **21**, 843 (2009).

[19] M. Sawicki, E. Guziewicz, M. I. Łukasiewicz, O. Proselkov, I. A. Kowalik, W. Lisowski, P. Dluzewski, A. Wittlin, M. Jaworski, A. Wolska, W. Paszkowicz, R. Jakiela, B. S. Witkowski, L. Wachnicki, M. T. Klepka, F. J. Luque, D. Arvanitis, J. W. Sobczak, M. Krawczyk, A. Jablonski, W. Stefanowicz, D. Sztenkiel, M. Godlewski, and T. Dietl, Phys. Rev. B **88**, 085204 (2013)

[20] T. Dietl, T. Andrearczyk, A. Lipińska, M. Kiecana, M. Tay, and Y. Wu, Phys. Rev. B **76**, 155312 (2007).

[21] L. T. Tseng, A. Suter, Y. R. Wang, F. X. Xiang, P. Bian, X. Ding, A. Tseng, H. L. Hu, H. M. Fan, R. K. Zheng, X. L. Wang, Z. Salman, T. Prokscha, K. Suzuki, R. Liu, S. Li, E. Morenzoni, and J. B. Yi, Phys. Rev. B **96**, 104423 (2017).

[22] Y. Matsumoto, M. Murakami, T. Shono, T. Hasegawa, T. Fukumura, M. Kawasaki, P. Ahmet, T. Chikyow, S. Koshihara, and H. Koinuma, Science **291**, 854 (2001).

[23] Y. Yamada, K. Ueno, T. Fukumura, H. T. Yuan, H. Shimotani, Y. Iwasa, L. Gu, S. Tsukimoto, Y. Ikuhara, and M. Kawasaki, Science **332**, 1065 (2011).

[24] H. Saadaoui, X. Luo, Z. Salman, X. Y. Cui, N. N. Bao, P. Bao, R. K. Zheng, L. T. Tseng, Y. H. Du, T. Prokscha, A. Suter, T. Liu, Y. R. Wang, S. Li, J. Ding, S. P. Ringer, E. Morenzoni, and J. B. Yi, Phys. Rev. Lett. **117**, 227202 (2016).

[25] P. N. Hai, L. D. Anh, S. Mohan, T. Tamegai, M. Kodzuka, T. Ohkubo, K. Hono, and M. Tanaka, Appl. Phys. Lett. **101**, 182403 (2012).

[26] P. N. Hai, L. D. Anh, and M. Tanaka, Appl. Phys. Lett. **101**, 252410 (2012).

[27] P. N. Hai, D. Sasaki, L. D. Anh, and M. Tanaka, Appl. Phys. Lett. **100**, 262409 (2012).

[28] N. T. Tu, L. D. Anh, P. N. Hai, and M. Tanaka, Jpn. J. Appl. Phys. **53**, 04EM05 (2014)

[29] N. T. Tu, P. N. Hai, L. D. Anh, and M. Tanaka, Appl. Phys. Lett. **108**, 192401 (2016).

[30] N. T. Tu, P. N. Hai, L. D. Anh, and M. Tanaka, arXiv:1706.00735 [cond-mat.mtrl-sci].

[31] B. Gu, and S. Maekawa, Phys. Rev. B **94**, 155202 (2016).

[32] Z. Xiao, F.-Y. Ran, H. Hiramatsu, S. Matsuishi, H. Hosono , and T. Kamiya, Thin Solid Films **559**, 100 (2014)

[33] A. Suter and B. M. Wojek, Phys. Procedia **30**, 69 (2012).

[34] A. S. Sefat, R. Jin, M. A. McGuire, B. C. Sales, D. J. Singh, and D. Mandrus, Phys. Rev. Lett. **101**, 117004 (2008).

[35] B. H. Toby and R. B. Von Dreele, J. Appl. Crystallogr. **46**, 544 (2013).

[36] A. Arrott, Phys. Rev. **108**, 1394 (1957).

[37] See Supplemental Material at [URL will be inserted by publisher] for Arrott plot and Seebeck effect measurments.

[38] T. Jungwirth, J. Masek, K. Y. Wang, K. W. Edmonds, M. Sawicki, M. Polini, Jairo Sinova, A. H. MacDonald, R. P. Campion, L. X. Zhao, N. R. S. Farley, T. K. Johal, G. van der Laan, C. T. Foxon, and B. L. Gallagher, Phys. Rev. B **73**, 165205 (2006).

[39] K. Y. Wang, K. W. Edmonds, R. P. Campion, B. L. Gallagher, N. R. S. Farley, C. T. Foxon, M. Sawicki, P. Boguslawski, and T. Diet, J. Appl. Phys. **95**, 6512 (2004).

[40] Z. Deng, K. Zhao, B. Gu, W. Han, J. L. Zhu, X. C. Wang, X. Li, Q. Q. Liu, R. C. Yu, T. Goko, B. Frandsen, L. Liu, J. Zhang, Y. Wang, F. L. Ning, S. Maekawa, Y. J. Uemura, and C. Q. Jin, Phys. Rev. B **88**, 081203(R) (2013).

[41] K. Zhao, B. Chen, G. Zhao, Z. Yuan, Q. Liu, Z. Deng, J. Zhu, C. Jin, Chinese Sci. Bull. **59**, 2524 (2014).

[42] Y. J. Uemura, T. Yamazaki, D. R. Harshman, M. Senba, and E. J. Ansaldo, Phys. Rev. B **31**, 546 (1985).

[43] S. R. Dunsiger, J. P. Carlo, T. Goko, G. Nieuwenhuys, T. Prokscha, A. Suter, E. Morenzoni, D. Chiba, Y. Nishitani, T. Tanikawa, F. Matsukura, H. Ohno, J. Ohe, S. Maekawa, and Y. J. Uemura, Nat. Mater. **9**, 299 (2010).

[44] F. L. Ning, H. Man, X. Gong, G. Zhi, S. Guo, C. Ding, Q. Wang, T. Goko, L. Liu, B. A. Frandsen, Y. J. Uemura, H. Luetkens, E. Morenzoni, C. Q. Jin, T. Munsie, G. M. Luke, H. Wang, and B. Chen, Phys. Rev. B **90**, 085123 (2014).

[45] K. Ahilan, T. Imai, A. S. Sefat, and F. L. Ning, Phys. Rev. B **90**, 014520 (2014).

[46] M. Sawichi, D. Chiba, A. Korbecka, Y. Nishitani, J. A. Majewski, F. Matsukura, T. Dietl, and H. Ohno, Nat. Phys. **6**, 22 (2010)

[47] L. Chen, F. Matsukura, and H. Ohno, Phys. Rev. Lett. **115**, 057204 (2015)

[48] L. Gluba, O. Yastrubchak, J. Z. Domagala, R. Jakiela, T. Andrearczyk, J. Żuk, T. Wosinski, J. Sadowski, and M. Sawicki, Phys. Rev. B **97**, 115201 (2018)

[49] M. Sawicki, O. Proselkov, C. Sliwa, P. Aleshkevych, J. Z. Domagala, J. Sadowski, and T. Dietl, Phys. Rev. B **97**, 184403 (2018)

[50] A. S. Sefat, D. J. Singh, R. Jin, M. A. McGuire, B. C. Sales, and D. Mandrus, Phys. Rev. B **79**, 024512 (2009).

[51] S. Haindl, M. Kidszun, S. Oswald, C. Hess, B. Buchner, S. Kolling, L. Wilde, T. Thersleff, V. V. Yurchenko, M. Jourdan, H. Hiramatsu, and H. Hosono, Rep. Prog. Phys. **77**, 046502 (2014).

[52] L. X. Cao, at Institute of Physics, Chinese Academy of Science. Private communications.